Supporting Information

Table S1. Variation in the viscosity with the PEO solution concentration.

Concentration (%)	8	14	18	22
Viscosity (Pa·s)	5.12	30.2	98.6	130.1

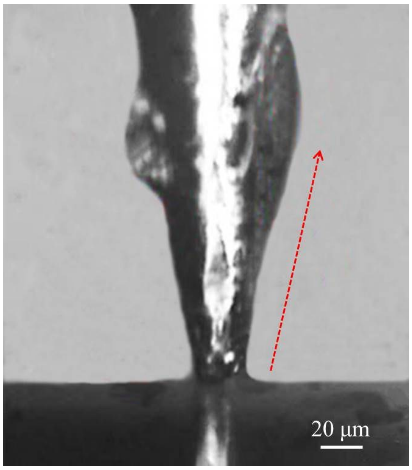

Figure S1. Optical images of the MWE with a fixed rod and a rotating solution tank (solution concentration: 10%, rotation speed: 720 r min^{-1})

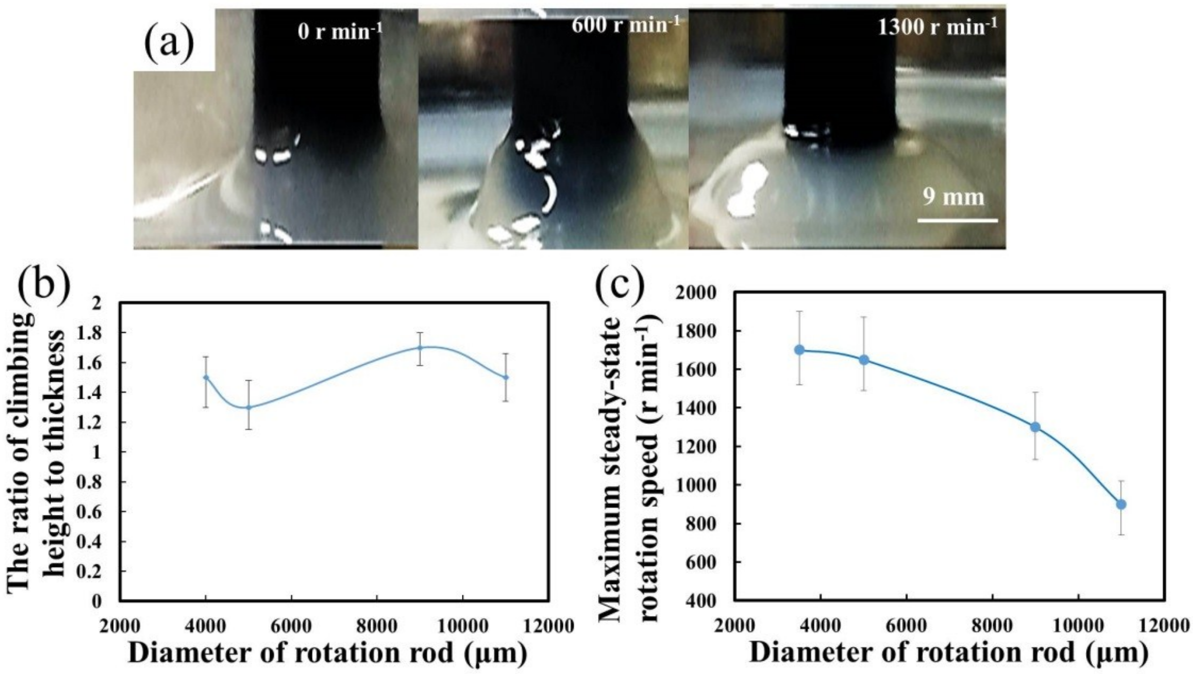

Figure S2. a) Optical images of rod-climbing behaviors under different rotation speeds of the rod with a diameter of 9 mm. b) Ratio of the climbing height to the thickness under the TWE (rotation speed: 600 r min^{-1}). c) Maximum steady-state rotation speed versus the diameter of the rod under the TWE. The solution concentration of PEO was 10% in a-c).

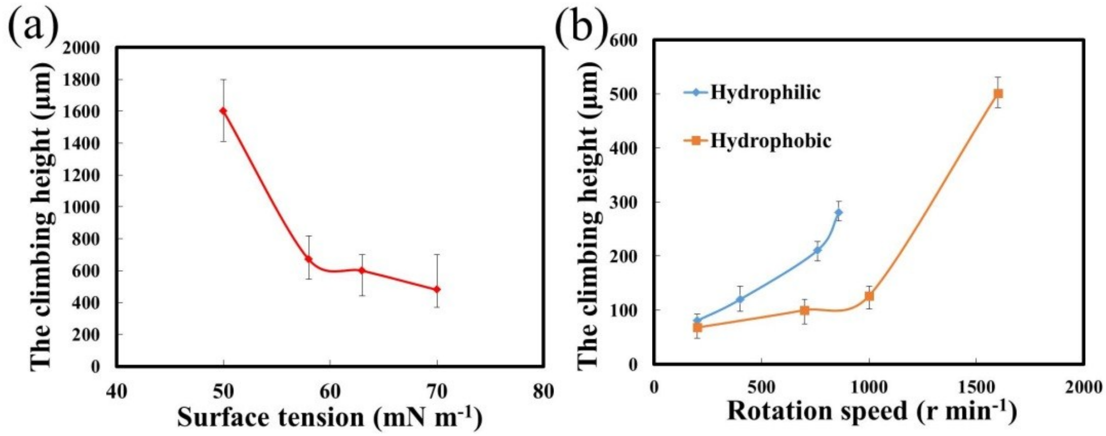

Figure S3. a) Climbing height under different surface tensions (solution concentration of PEO: 12%, rotation speed: 650 r min^{-1}). b) Climbing height after hydrophobic treatments under different rotation speeds (solution concentration of PEO: 10%). The diameter of the rotation rod was 200 μm in a-b).

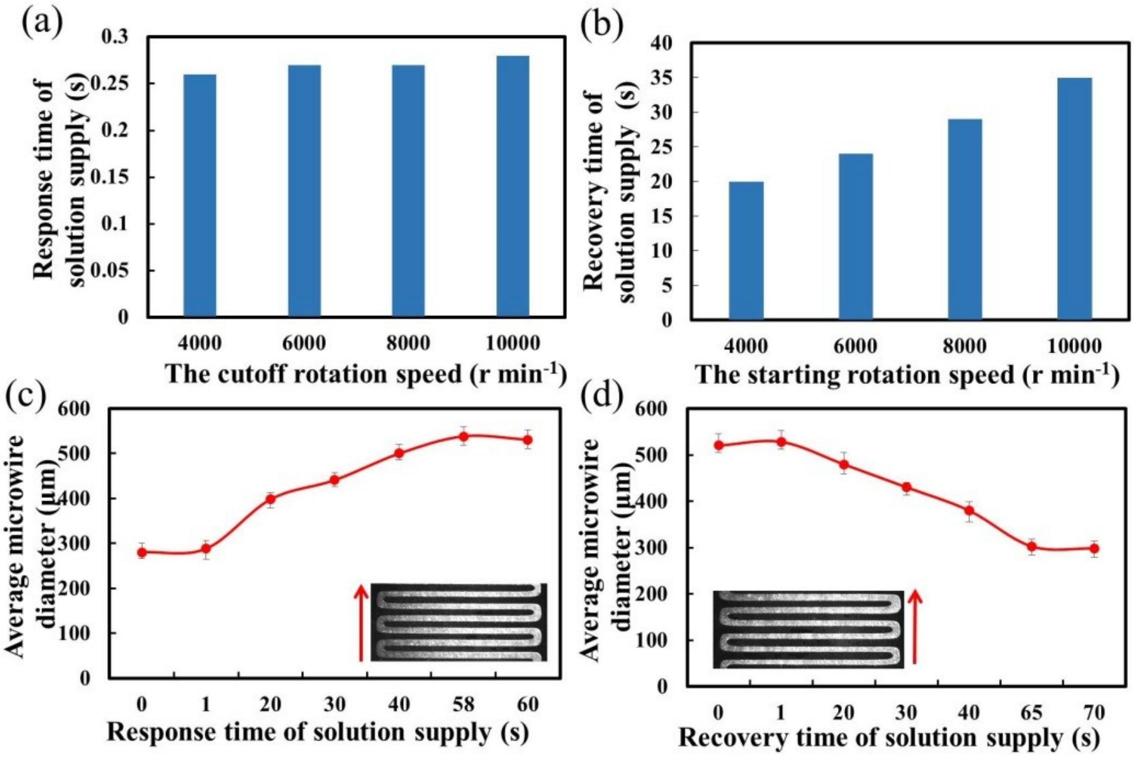

Figure S4. a) The response time of solution supply varied with different cutoff rotation speeds. b) The recovery time of the solution supply varied with different initial rotation speeds. c-d) Response and recovery times of the solution supply based on a high-precision injection pump. The length of the rotation rod tip extending out of the steel capillary, the distance from the rod tip to the collector, the collector moving speed and solution concentration of PEO were 118 μm, 23 μm, 1 mm s^{-1} and 18%, respectively.

Double-rod-climbing Phenomenon to Enhance Pumping properties

The above results suggest that we can utilize the MWE to pump a high-viscosity solution at the picoliter level. However, our experiments demonstrated that the raised solution breaks the bondage from surface tension and flows down the outside of the raised column of solution due to the higher centrifugal force when the rotation speed exceeds a certain value, which would decrease the stability in the pumping solution. Moreover, we fixed a rod near the rotation rod to enhance the rod-climbing effect (**Figure S5a**), because the fixed rod near the rotation rod can provide a higher shear rate for the edge of the raised column of solution.[30] Clearly, the solution near the rod can quickly climb to the top of the rod to a height far above the climbing height observed without the fixed rod (**Figure S5b**). **Figure S5c** shows that varying the distance between the fixed rod and the rotation rod can change the climbing height. When the distance is more than 100 μm, the transport of the solution is very unstable, and a bubble-like phenomenon occurs. Thus, the optimal distance is less than 100 μm. By comparing the double-rod-climbing phenomenon under the MWE (Figure S5b) and TWE (Figure S6), we can conclude that the double-rod-climbing phenomenon is a special microscale phenomenon, which can be used for solution pumping. Compared to the micro/nanopipe, the pump based on MWE can decrease the high solution resistance from the micro/nanochannel, so the maximum pumping height with MWE is over 6 mm under double-rod-climbing conditions **Figure S5d**. The results in Figure S5b-c suggest that these phenomena are results of the MWE. Although the minimum distance between the fixed rod and the rotation rod is 100 μm in our experiments, the minimum thickness of the raised column of solution was less than 1 μm in Figure S5b. This finding indicates that this pump can be used at the microscale in the future. Furthermore, we also find that the twisted rotation rod, which is difficult to rotate under the TWE, can also transport highly viscous solutions.

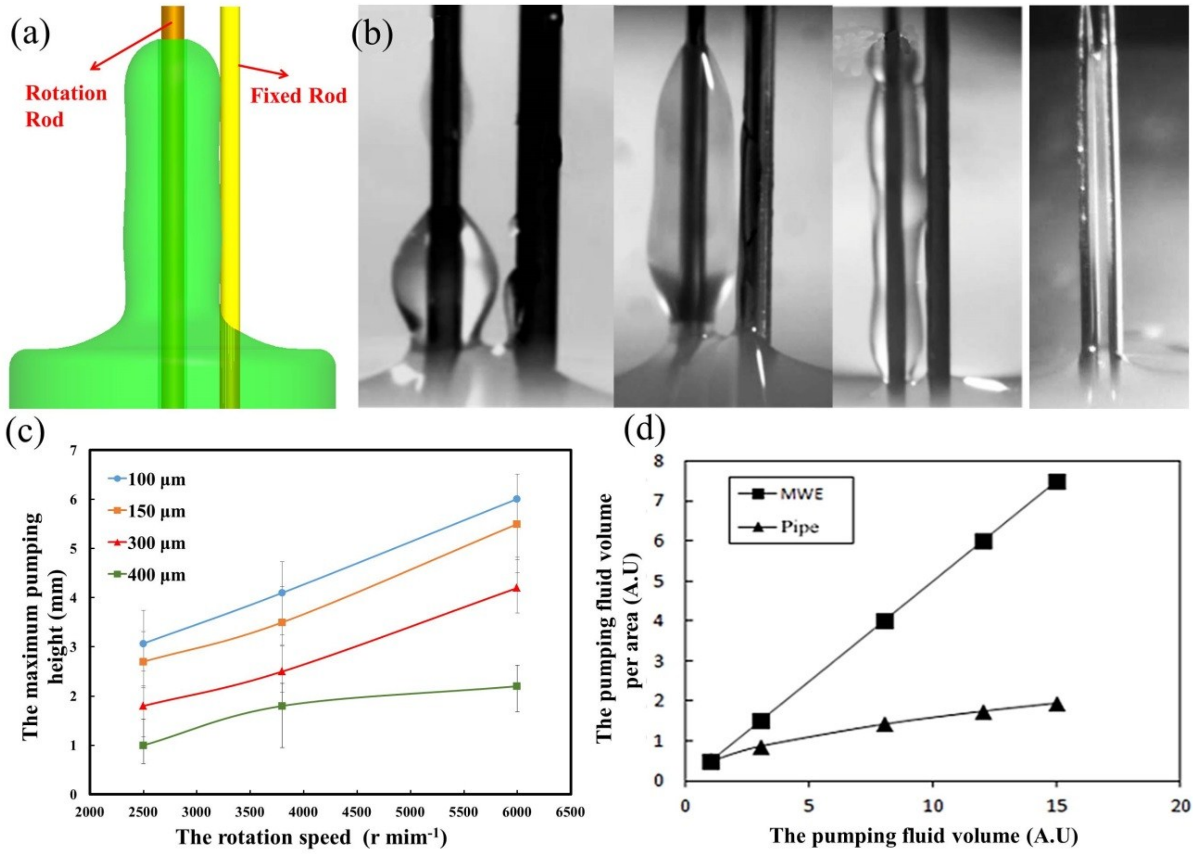

Figure S5. Double-rod-climbing phenomenon. a) Schematic diagram of the double-rod-climbing phenomenon. b) Optical images of double-rod-climbing phenomenon with different distances between the rotation rod and the fixed rod (distances: 400 µm, 300 µm, 150 µm and 100 µm, rotation speed: 4850 r min^{-1}). c) Maximum pumping height with different distances versus rotation speed. d) The pump efficiency for different pumps. The PEO solution concentration, the rotation rod diameter and diameter of the fixed rod were 10%, 200 µm and 300 µm, respectively.

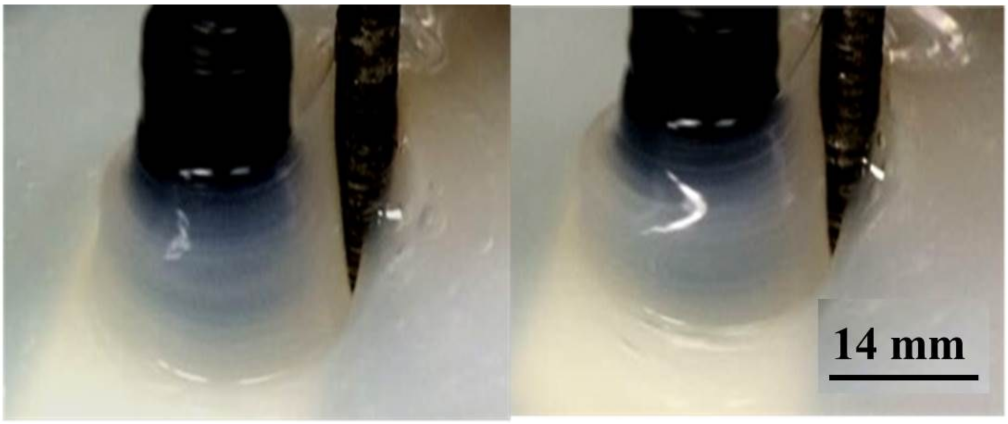

Figure S6. Optical images of the double-rod-climbing phenomenon under the TWE (solution concentration of PEO: 10%, rotation speed: 2870 r min^{-1}).

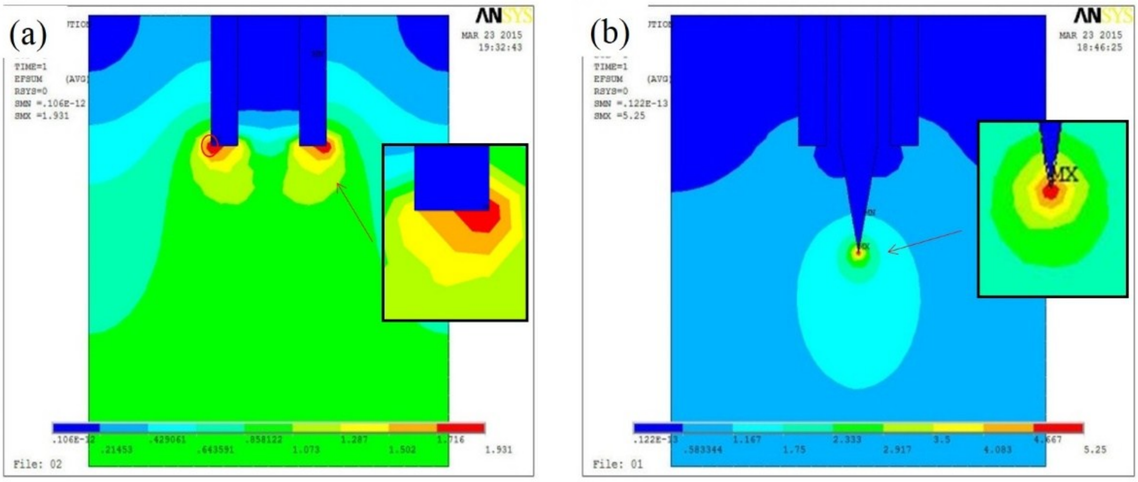

Figure S7. Electric field simulation near the nozzle in direct writing with a) A hollow nozzle; b) MWE.

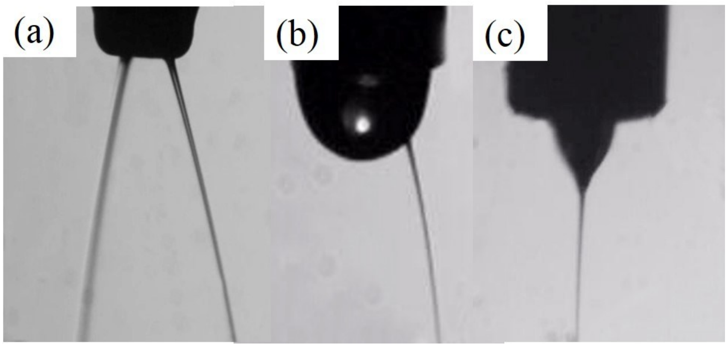

Figure S8. Optical images of jet in direct writing process. a) and b) printing with a hollow nozzle. c) printing with MWE.

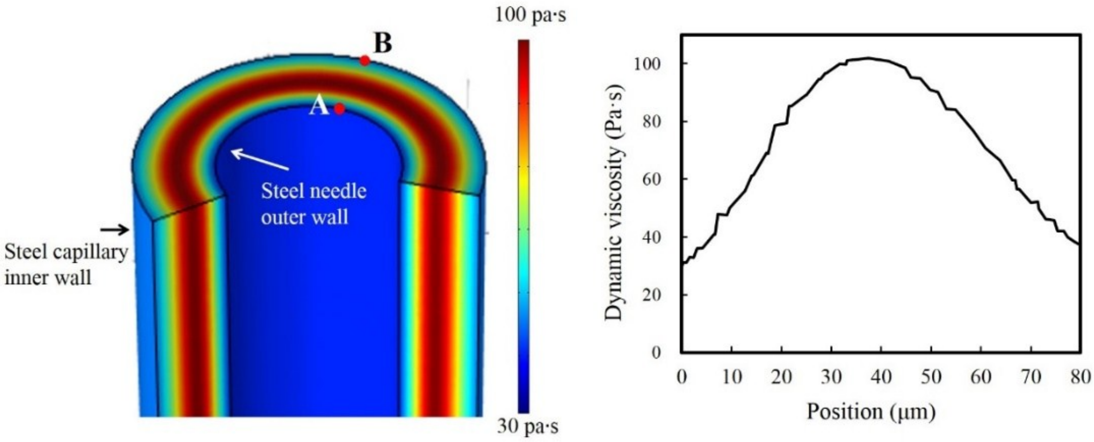

Figure S9. Simulation of solution viscosity in the microchannel in MWE based direct writing.

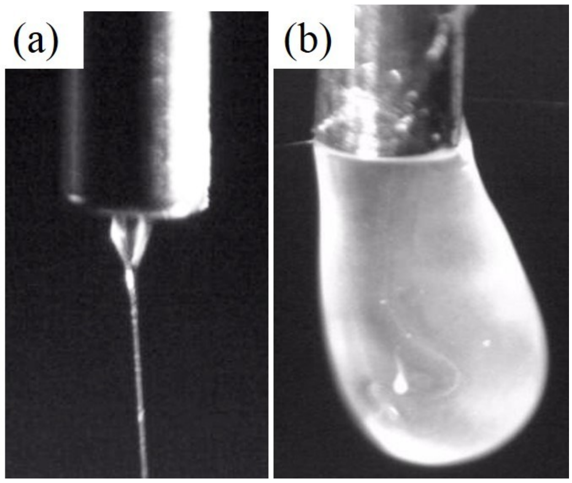

Figure S10. Optical images of a) a jet during MWE based direct writing with an applied voltage and b) a droplet pendent of spinneret in direct writing with hollow nozzle.

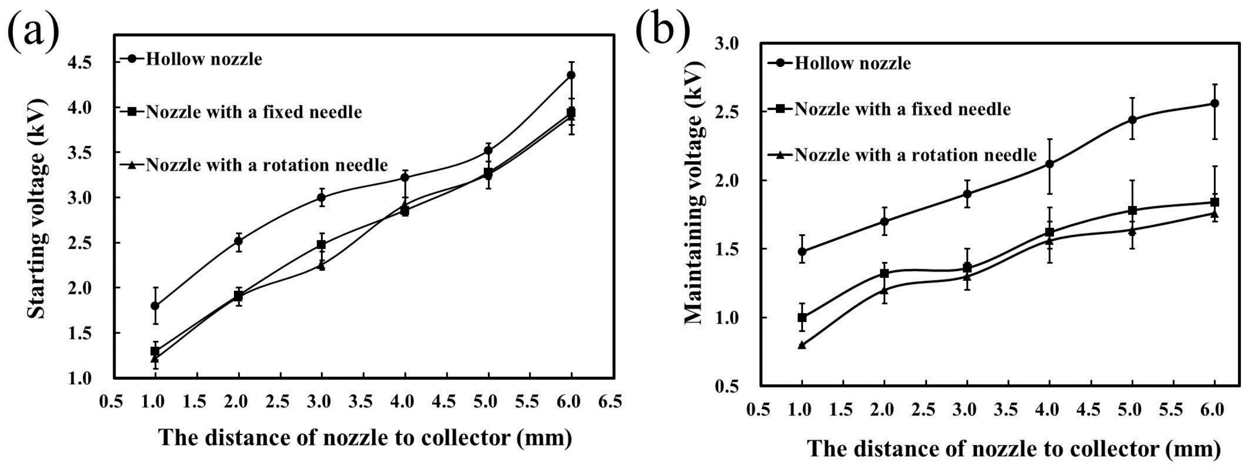

Figure S11. a) The initial voltages vary with the distance from the nozzle to the collector with different types of nozzles. b) The maintaining voltages vary with the distance from the nozzle to the collector with different types of nozzles.

Pumping volume measurement.

When the time goes from t_1 to t_2, the volume increases from V_1 to V_2. So the time interval is:

$$\Delta t = t_2 - t_1 \tag{1}$$

The pumping volume during the time (Δt) is:

$$\Delta V = V_2 - V_1 \tag{2}$$

So the solution flow rate (Q) is:

$$Q = \frac{\Delta V}{\Delta t} \tag{3}$$

The volume change cannot be directly measured, so we used a CCD camera to record the solution changing process at the tip of the needle, KMplayer Plus software was used to intercept a series of images (The start time is t_1, the end time is t_2, Figure S12a). Then we used Pro/Engineer 3D software to model the droplet images at t_1 and t_2 moments (Figure S12b) and the volume of v_1 and v_2 could be automatically calculated. To analysis the error, we collected 50 data at a time, and the measurement error was about 18pL. So the minimum pumping volume was also measured by this method.

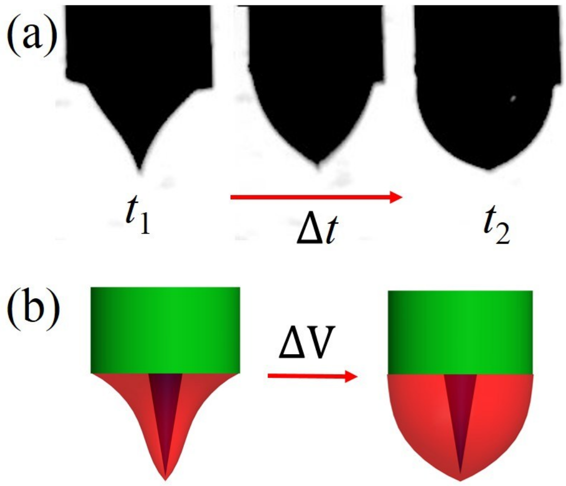

Figure S12. a) Images of droplet at the tip of needle. b) Models of droplet.